A micro coordinate measuring machine using an active stereovision technique for measuring 3D micro parts

M. U. Khan, E. Dupont, H. Al-Hajjar, C. Mattar, Christine Prelle, F. Lamarque

Available online at www.sciencedirect.com

ScienceDirect

IFAC Papers Online CONFERENCE PAPER ARCHIVE

IFAC PapersOnLine 50-1 (2017) 8648–8653

A micro coordinate measuring machine using an active stereovision technique for measuring 3D micro parts ⋆

M.U. Khan * **E. Dupont** * **H. Al-Hajjar** * **C. Mattar** * **C. Prelle** * **and F. Lamarque** *

* *Roberval Laboratory - UMR 7337, Sorbonne universités, Université de Technologie de Compiègne (UTC), Compiègne, CS 60203 France, (e-mail: muneeb-ullah.khan@utc.fr, erwan.dupont@utc.fr, hani.al-hajjar@utc.fr, charbel.mattar@etu.utc.fr, christine.prelle@utc.fr, frederic.lamarque@utc.fr).*

Abstract: This paper presents a micro coordinate measuring machine capable to measure and reconstruct three dimensional surfaces of micro parts. The uniqueness of the proposed machine lies in its small foot print with ability to displace micro objects beneath the measuring probe for continuous surface characterisation with micrometer level resolution. Its miniature measuring probe enables its easy integration into several micro applications. In addition, the multiple surface stitching algorithm used in the micro-coordinate measuring machines enhances its capability to reconstruct and measure large 3D surfaces.

Keywords: Electromagnetic devices, Positioning systems, Image reconstruction, Image modeling, Image analysis, Optical spectroscopy.

1. INTRODUCTION

Nowadays, Coordinate Measuring Machines (CMMs) are widely adopted in numerous manufacturing industries such as aeronautics, automobile, etc., to achieve high quality and precision standards in manufacturing and assembly processes of three-dimensional mechanical components. The distinct ability of these machines to measure geometrical parameters of the tridimensional mechanical parts or assemblies against the design intent, has greatly revolutionized current mechanical products to meet high quality manufacturing standards, Sudatham et al. (2015).

In general, CMMs are typically used with contact sensors (i.e., measurement probe) to retrieve physical measurements of the mechanical parts and/or assemblies. In practice, these CMMs delivers high accuracy and repeatability during measurement. However, due to their contact-type measurement approach, their application to measure small mechanical pieces having volume from few cubic micrometers to few cubic millimeters is limited, Yang et al. (2011). This is mainly due to the difficulties such as deterioration of small mechanical parts as a result of the measurement probe's contact during physical measurement, the limited measurement resolution due to the size of the measurement probe used in the contact-type CMMs, etc.

In order to solve the aforementioned constraints, contactless CMMs based on optical technology (i.e., interferometry, triangulation, stereo imaging based on structured light, etc.) are often employed to measure mechanical parts having small volume. The advantages of contactless CMMs is twofold. First, no additional geometrical information is needed regarding the mechanical part prior to the measurement, and second, it delivers fast measurements by eliminating the need of point-by-point measurements as essential in contact-type CMMs.

Apart from the advance features incorporated into the contactless CMMs, their huge size and excessive energy consumption for measuring micro mechanical parts yield an expensive solution. In addition, the ever-growing micro factory concept introduced in 1990, to economize the low and mid-volume production cost of the customized products, has led to great challenges by miniaturize pre-exiting conventional machines, e.g., milling machine, drilling machine, etc., Hofmann et al. (2011); Siltala et al. (2011); Kobel and Clavel (2011). So, being an essential device of the current high quality production environment, the downsizing of typical contactless CMMs demands innovative technological solutions to miniaturize various components (i.e., actuation platform, measurement probe, feedback control, etc.) without diminishing their output characteristics such as measurement resolution, measurement speed, etc.

In this paper, a Micro Coordinate Measuring Machine (μCMM) prototype capable to measure small mechanical piece and reconstruct its 3D image is presented. The planar actuator of the μCMM is able to move a miniature mechanical piece beneath the contactless measurement probe in horizontal plane. The measurement probe takes multiple images during actuator's movement and reconstructs a long surface of the piece using image stitching technique. In addition, during reconstruction process, the planar ac-

⋆ This work is realized under the MICROCOSM project and supported by the Picardie region and co-financed by Europe/FEDER with the European funds for regional developments at Picardie region of France.

10.1016/j.ifacol.2017.08.1522

tuator can easily position the mechanical piece beneath the measurement probe to take high quality measurement with respect to the information deduced via image processing. In second section, the description of the μCMM is provided. In the third section, planar actuator is discussed and 3D measurement system and the used image stitching technique is presented in the fourth section. At the end conclusion and perspective is provided.

2. DESCRIPTION OF MICRO COORDINATE MEASURING MACHINE

The proposed μCMM consists of a planar actuation system, a 3D measurement system and an Input/output hardware and software control modules as depicted in the Fig.1. The planar actuation system includes a planar electromagnetic actuator capable to displace a specimen (i.e., mechanical piece, etc.) beneath the measurement probe. In addition, a position control unit manages the motion of the planar actuator to achieve desired trajectories in horizontal plane.

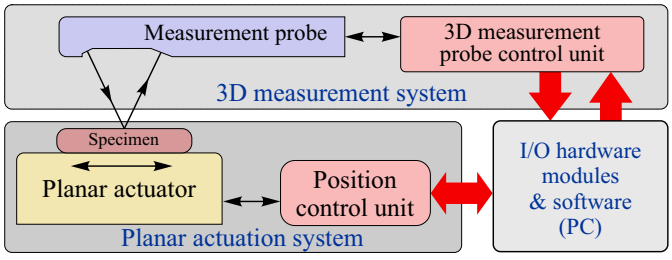

Fig. 1. Schematic layout of the μCMM.

The 3D measurement system of the μCMM consists of a active stereovision principle based measurement probe as shown in the Fig.2. A dedicated 3D measurement probe control unit handles the functioning of the measurement probe by projecting the structured light and measuring the pattern's distortion on a small objects such as a euro coin as shown in the Fig.2. The I/O hardware and software modules integrated in a Personal Computer (PC) assist in generating the desired motion trajectories for the planar actuator and analyze the measured information from measurement probe. In order to realize a long measured surface, the software modules combines complex algorithms to stitch measured surface data. The detail description of these components is provided in the following sections.

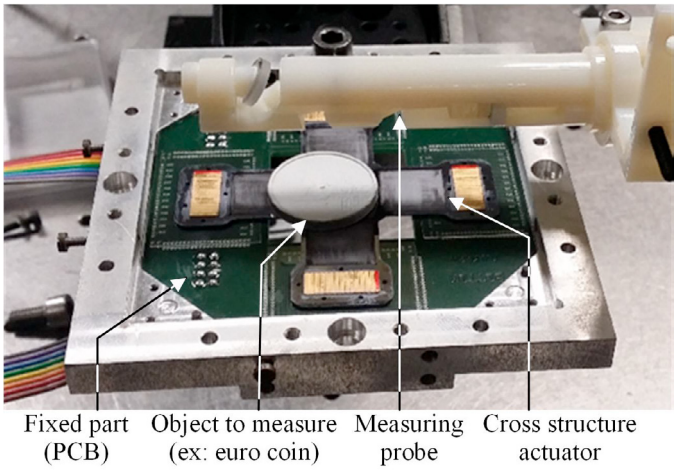

Fig. 2. Real view of the compact μCMM prototype.

3. PLANAR ACTUATOR

The planar actuator of the μCMM consists of a mobile part and a fixed part, see Fig. 3. The mobile part integrates Permanent Magnet Arrays (PMAs) into a light weight microfabricated silicon cross structure, see Khan et al. (2010). A single PMA consists of a set of 14 Permanent Magnets (PMs) in North-South (NS) configuration. The dimensions of each PM are $1\,\text{mm} \times 1\,\text{mm} \times 6\,\text{mm}$ and provide a remanent magnetization of 1.43 T along z-axis. The NS pole configuration helps in self-assembly of the PMs without needing any bonding agent, see Khan et al. (2012).

The fixed part of the planar actuator, having dimensions of $80\,\text{mm} \times 80$ mm, consists of a pair of Planar Drive Coils (PDC) along x-axis and y-axis in xy-plane. A single PDC includes two copper coils for routing two phase driving currents (I_1 and I_2), independently. The fixed part has been fabricated into 1.5 mm thick double side FR4 printed circuit board. In addition, to achieve smooth motion surface and insulation between the mobile and fixed part of the planar actuator, each PDC is covered with a 130 μm thick flat glass layer.

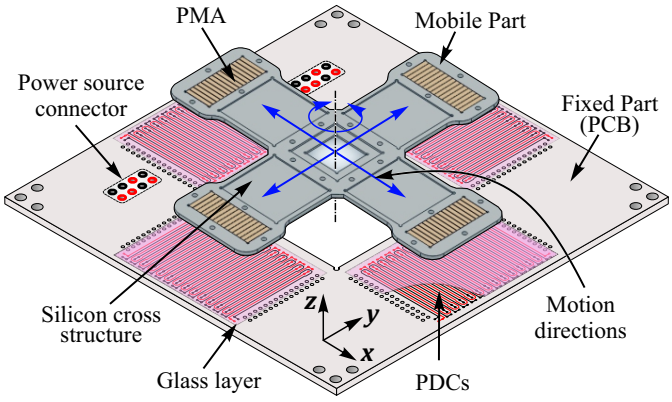

Fig. 3. Three dimensional model of the planar actuator.

In the planar actuator design, the combination of each PMA facing corresponding PDC, acts as a Linear Motor (LM). From Fig.3, it can be seen that two orthogonally arranged pairs of the LMs in xy-plane aid to translate and rotate the mobile part of the planar actuator over the fixed part about its central axis in xy-plane.

3.1 Working principle of the planar actuator

The working principle of each LM of the planar actuator is based on the generation of the Lorentz forces. When sinusoidal currents are injected into the fixed PDCs of the LM, a Lorentz force appears over each PMA due to the interaction between the magnetic field from the PMs and currents in the PDCs. The resulting electromagnetic force tends to translate the mobile part (i.e., PMA) over the fixed part (i.e., PDC covered with glass layer). The translation force (F_x) and leviation force (F_z) are the

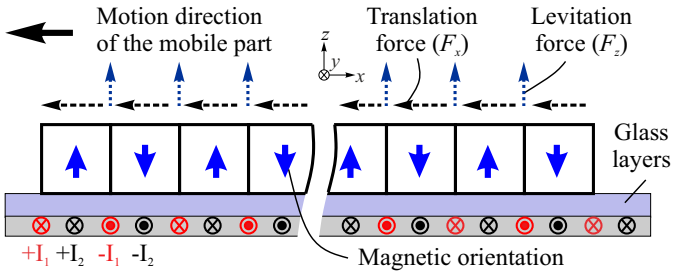

Fig. 4. Working principle of the planar actuator.

electromagnetic force components that drive and levitate the mobile part, respectively, see Fig.4. In order to achieve continuous motion, the phase difference between the injected currents (I_1 and I_2) is kept at $\pi/2$. Furthermore, to achieve forward (i.e. along $+x$-axis) and backward (i.e. along $-x$-axis) motion along x-axis, the phase difference of the injected currents is changed from $+\pi/2$ to $-\pi/2$, see Khan et al. (2012).

In order to achieve multiple precise measurements of the micro object, the motion path of the planar actuator needs to be controlled using non-contact feedback displacement sensors, see Prelle et al. (2006). In addition, by adopting a closed loop control for the planar actuator, the planned motion trajectories can be achieved with nanometer level precision, see Khan et al. (2016). However, in order to validate the concept and minimize the experimentation time, the motion of the planar actuator have been realized with open-loop control in this study. For this, the pre-planned motion path of the actuator has been generated by sampling the desired millimetric xy-displacement trajectory with 10 μm step resolution. Based on the obtained displacement trajectory samples, the regulated sinusoidal currents (i.e., $I_1 + \Delta I_1$ and $I_2 + \Delta I_2$) with respect to the actuator's position, are injected into PDCs to drive the mobile part of the planar actuator to the desired position on the motion trajectory. For our initial study, this approach aids in achieving complex motion trajectories (e.g., circular, square, etc.) in xy-plane without implementing feedback sensors. However, in future, a feedback displacement sensor that is essential to realize motion trajectories with nanometer level positioning resolution will be implemented in the planar actuation system.

4. 3D MEASUREMENT SYSTEM

In this section, the detail description of the 3D measurement system along with its measurement principle and point cloud fusion technique is discussed.

4.1 Measurement probe architecture

The 3D measurement system consists of a miniaturized measurement probe. Its architecture is presented in Fig. 5, see Hou et al. (2014). The measurement principle is based on active stereovision that takes the projection of structured light patterns on the object to be analyzed into account. The measurement and analysis of the patterns's distortion lead to the reconstruction of 3D object shape.

In order to design an active stereovision system, the device is divided in two channels. The first is the projection

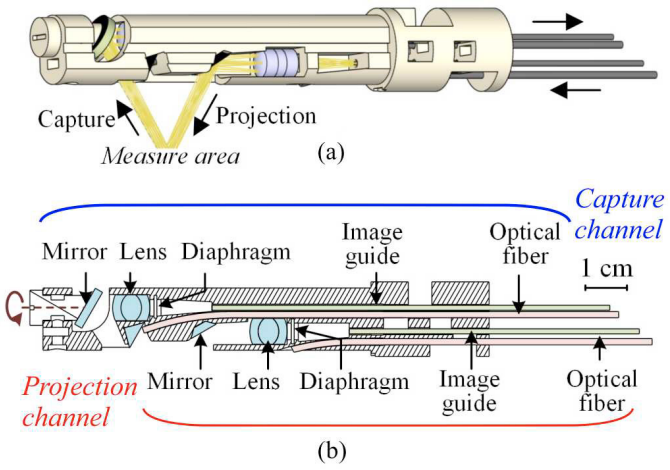

Fig. 5. (a) 3D CAD model of the measurement probe. (b) Cross section view of the measurement probe architecture displaying internal components.

channel where a pattern is generated and focused on the measured object, and the second is the capture channel where a camera measure the projected pattern image. A triangulation angle between the two channels encodes the depth information.

To develop the measurement system, the projecting and capturing opto-electronic devices are optically connected to the 2 m long image guides (FIGH-70-1400N, Fujikura Inc.). Each image guide consists of a fiber bundle having 70000 optical fibers within a total diameter of 1.4 mm.

Furthermore, to generate the projected patterns, a Digital Micro-mirror Device (DMD), fabricated by Texas Instrument Inc, is used. This is a MEMS device composed of 1024×768 squared mirrors of 10.8 mm pitch. A white light source is used to illuminate the DMD. This light is structured and injected into the first image guide. The light received from the other end of the first image guide is then projected through a Triplet Steinhel lens, a mirror and finally focused on the desired area to be measured. Afterwards, the structured light patterns reflected from the measured object area are re-injected into a second image guide (identical to the first) through the capture channel composed of a mirror and a Triplet Steinhel lens as shown in Fig. 5(b). Finally, the other end of the second image guide is optically connected to a CCD Camera (Flea 2 Camera, Point Grey Inc.), where the image of the object to measure and the projected patterns are captured.

Using this miniaturized measurement probe, a time multiplexed patterns sequence is projected on the object to measure it, as explained on the following subsection.

4.2 3D measurement principle

The 3D measurement principle used to reconstruct the object shape is based on a time multiplexing method adapted for structured light projection, also named as phase shifting, see Salvi et al. (2010). In this method, a sequence of vertical sinusoidal patterns are projected. And between each pattern, the signal phase is shifted by small increments. For each pixel of the camera sensor, the phase detection allows to calculate one 3D point coordinate and

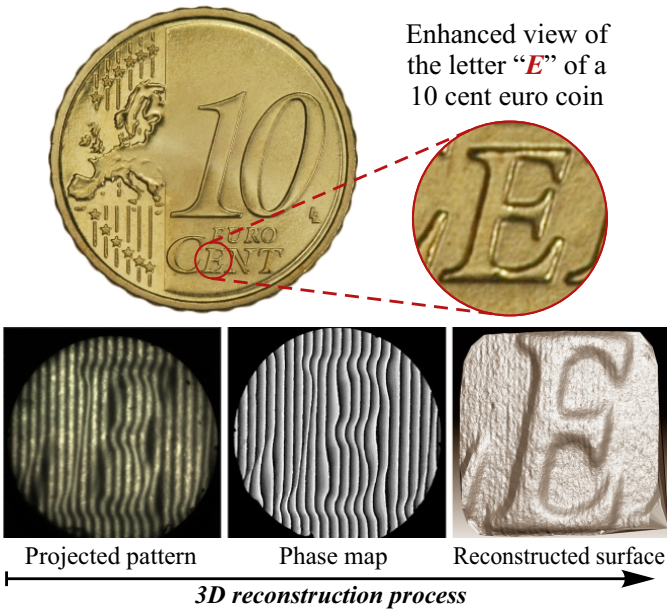

Fig. 6. 3D reconstruction of the letter "*E*" of a 10 cent euro coin based on a phase-shifting principle.

for the whole sensor, a global height map representing the measured surface is calculated, see Fig. 6.

The intensity of each captured pixel is calculated using (1).

$$I_i(x,y) = L_p(x,y)\sin(\varphi(x,y)+\delta_i) + L_a(x,y) \qquad (1)$$

Where x and y are the pixel coordinates of the i^{th} captured image. L_a is the intensity due to the ambient lighting, L_p is the intensity due to the projection lighting. δ_i is the phase of the i^{th} pattern and the $\varphi(x,y)$ phase encodes the 3D depth information for the pixel (x,y). For N phase shifting, the value of the phase φ can be computed using (2).

$$\varphi(x,y) = \tan^{-1}\left(\frac{-\sum_{i=1}^{N} I_i(x,y)\sin(\delta_i)}{\sum_{i=1}^{N} I_i(x,y)\cos(\delta_i)}\right) \qquad (2)$$

Next, a phase unwrapping method is applied on $\varphi(x,y)$ and this unwrapped phase is finally converted into a 3D coordinate value using the system calibration. Finally, a 3D point cloud representing the measured area shape is calculated. Once a 3D reconstruction process is finished, the following step is to move the planar actuator to measure a second area adjacent to the first one. Each measured area need to overlapped with the precedent one, so that it can be algorithmically aligned to stitch multiple measurements. This 3D stitching principle results in acquiring the whole surface of the object.

4.3 Point cloud fusion

4.3.1. Surface stitching principle

The concept of stitching elements with their overlapping fields was first introduced for 2D panoramic imaging with two or more images and was then applied in the 3D scope with surface stitching. The goal of this method is to find the position and orientation of 3D point clouds in a global coordinate system, such that the intersecting areas between the point clouds overlap perfectly.

The 3D stitching process is divided into three main steps which are key-point detection, registration and estimation of the final transformation. Firstly, for the key-point detection algorithm, an appropriate mathematical model is needed to associate effective 3D points from one surface to the other so that the matching features can be determined easily. These associated 3D points are called correspondences. They are used in the registration process to search for surface alignments that minimizes the overall sum of distances between corresponding 3D points. Then, a transformation estimation is applied to align the two consecutive point clouds into a single wider surface.

4.3.2. Iterative Closest Point with Normal method

In order to determine the overlapping parts in the point cloud pair data acquired via two measures, corresponding features must be found. For X,Y and Z coordinates used as the only features to compare the point cloud pair data, nearest neighbor search method can be applied. Using this principle, one popular method is the Iterative Closest Point (ICP) method (see Salvi et al. (2007)) which consists of iteratively applying estimation and error reduction algorithms to finally align two point clouds into one final model. The ICP method minimize a weighted sum of squares of the distances between the source data points and the target corresponding closest points.

An efficient variant of ICP is named ICPN (Iterative Closest Point with Normal) and based on point-to-plane minimization. In addition of the three coordinates points in R^3 used by ICP, the ICPN algorithm also handles the surface normal values. The purpose of this specific algorithm is to minimize the squared distance sum between the first cloud source points and the tangent plane at its corresponding target point on the second cloud. Both, ICP and ICPN methods were tested experimentally in our study and ICPN proved to be more precise although slower than ICP.

4.3.3. Result of stitching using ICPN method

The registration algorithm was experimentally tested with the 3D probe (see paragraph 4.1) on a 10 cent euro coin as shown in Fig. 7. From the results, it can be observed that two overlapping surfaces were reconstructed one after the other. Each 3D measure of point clouds contains around 308000 points, covering an elliptic area of 2.4 mm×2.2 mm and a total depth of 0.8 mm. Hence, the average density of the acquired point cloud is 70000 points per millimeter.

The 3D rendering of the measured two point clouds stitching is illustrated in Fig. 8(a). A horizontal section of the point clouds stitching is presented in Fig. 8(b). Furthermore, the results of the error distance between the two point clouds are shown in Fig. 8(c). The ICPN registration process computation time was found to be 87.4 seconds using an Intel Xeon E5-1620 processor with 8 cores each having 3.60 GHz frequency. Moreover, the average error on the measured profile between the two point clouds is found to be 1.65 μm with a standard

Fig. 7. Measurement of two parts on a 10 cent euro coin, i.e., the first part measure half of the letters "N" and "T", and the second part measure the full letter "T".

deviation of 1.04 μm. The computation time can be further reduced by optimizing certain parameters such as down-sampling the input and output point clouds, making the algorithm efficient by exploiting the multi-threaded feature of all processor cores, etc.

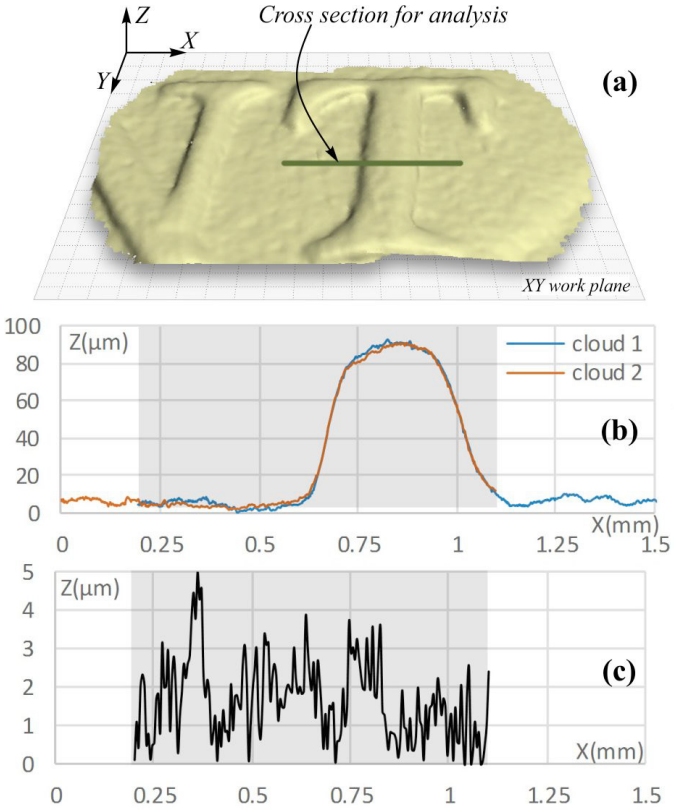

Fig. 8. (a) Rendering of a point cloud resultant from an ICPN pair-wise registration. (b) Horizontal profile section of the point clouds. (c) Absolute error between the two consecutive point clouds.

4.3.4. Automatic registration algorithm

After the stitching process, an automatic registration algorithm is developed to align multiple point clouds, one after the another to cover the whole measured surface. The algorithm inputs are the point clouds data files and the displacements values. Using the developed algorithm, 16 point clouds with a total of 4931243 3D points are aligned in 839 seconds using an ICPN method, see Fig. 9.

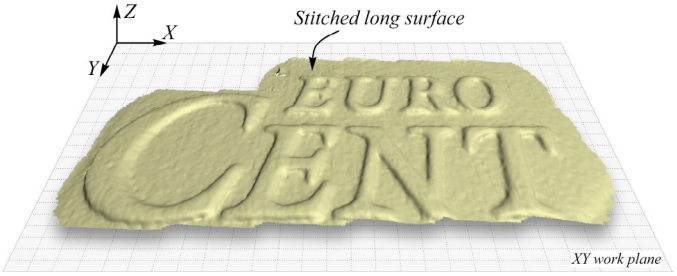

Fig. 9. Rendering of the 16 3D measures after the automatic registration process using ICPN method.

4.3.5. Control of actuator using point cloud information

Currently in this μCMM, the 3D measurements and actuation are applied in open-loop ,i.e., the object trajectory under the 3D probe is defined prior to the measurement process and according to the shape of the object to measure. Once all measurements are done, the final 3D surface is computed by merging all the acquired 3D points using the stitching method. In addition, the measurement error due to the open loop control is compensated during merging of 3D points via the stitching algorithm.

The architecture of the μCMM allows a closed-loop control of the measurement as illustrated in Fig. 1. At the end of each 3D reconstruction, the measurement quality can be evaluated. If the result is not satisfying due to noise, occlusions, holes in the reconstruction surface, etc., the actuator can moved to a position that could potentially give a better result quality and the measurement process is carried once again. Consequently, the 3D reconstruction results can be used as a control feedback on the μCMM to better position the object bellow the 3D probe in order to optimize the final point cloud resolution.

Another closed-loop feature obtained with this μCMM architecture is related to the 3D probe capability to operate as a position sensor. Indeed, each time a stitching process end, a transform matrix between the last 3D measurement and the previous one is obtained. This transform matrix describes the object movement, in translation and rotation with respect to the last displacement of the actuator. This matrix can be used as feedback data to control the planar actuator displacement. It can also be a way to validate the data coming from the position sensor already integrated into the planar actuator.

5. CONCLUSION AND FUTURE WORK

In this work, a compact design of a μCMM to measure small mechanical parts is presented. The small foot print (i.e., 80 mm×80 mm) of the μCMM makes it suitable for easily integrating it into small working space. In addition, the high speed dynamics and 3DOF motion capability of the electromagnetic planar actuator enhances its ability to precisely position the small objects for analysis beneath the measurement probe with micrometer level resolution.

In addition, a 3D probe using active stereovision was designed to measure elliptic areas of 2.4×2.2 mm^2 over a depth of 0.8 mm with a micrometer level resolution and based on a phase-shift reconstruction algorithm. In order to measure larger areas than the probe field of

view, a stitching method using an Iterative Closest Point with Normal (ICPN) algorithm was used to align all measured surfaces together. Experimental measurements were applied on a 10 cent euro coin and the mean error value of the alignment between two overlapping surface was found to be 1.65 μm. A total of sixteen point clouds were finally aligned using the ICPN algorithm.

In future, we planned to implement a control feedback on the planar actuator using the position and orientation values provided by the stitching algorithm. Also, the 3D reconstruction results will be analyzed during the measuring process and used as an input to adopt the planar actuator trajectory in order to optimize the final 3D point cloud quality. Furthermore, dedicated position control algorithms will be developed and integrated into the developed stitching algorithm while optimizing measurement parameters such as, measurement speed, etc.

REFERENCES

Hofmann, A., Hummel, B., Firat, O., Bretthauer, G., Br, M., and Meyer, M. (2011). microflex - a new concept to address the needs for adaptable meso and micro assembly lines. In *Assembly and Manufacturing (ISAM), 2011 IEEE International Symposium on*, 1–5.

Hou, Y., Dupont, E., Petit, L., Redarce, T., and Lamarque, F. (2014). Dynamic reconfiguration of a compact active stereovision system with digital electromagnetic actuators. In *2014 IEEE/ASME International Conference on Advanced Intelligent Mechatronics*, 1128–1133. IEEE.

Khan, M.U., Bencheikh, N., Prelle, C., Lamarque, F., Beutel, T., and Buttgenbach, S. (2012). A long stroke electromagnetic XY positioning stage for micro applications. *Mechatronics, IEEE/ASME Transactions on*, 17(5), 866–875.

Khan, M.U., Prelle, C., Lamarque, F., Beutel, T., and Bttgenbach, S. (2010). Silicon conveyor based planar electromagnetic device for linear displacement. In *2010 IEEE/ASME International Conference on Advanced Intelligent Mechatronics*, 231–236.

Khan, M.U., Prelle, C., Lamarque, F., and Buttgenbach, S. (2016). Design and assessment of a micro positioning system driven by electromagnetic actuators. *IEEE/ASME Transactions on Mechatronics*. doi: 10.1109/TMECH.2016.2613548.

Kobel, P. and Clavel, R. (2011). Micro robot for rotary desktop assembly line. In *Assembly and Manufacturing (ISAM), 2011 IEEE International Symposium on*, 1–6.

Prelle, C., Lamarque, F., and Revel, P. (2006). Reflective optical sensor for long-range and hig-resolution displacements. *Sensors and Actuators A: Physical*, 127(1), 139–146.

Salvi, J., Fernandez, S., Pribanic, T., and Llado, X. (2010). A state of the art in structured light patterns for surface profilometry. *Pattern recognition*, 43(8), 2666–2680.

Salvi, J., Matabosch, C., Fofi, D., and Forest, J. (2007). A review of recent range image registration methods with accuracy evaluation. *Image and Vision computing*, 25(5), 578–596.

Siltala, N., Prusi, T., Vuola, A., Heikkil, R., and Tuokko, R. (2011). Modular microfactory system for gas sensor assembly. In *Assembly and Manufacturing (ISAM), 2011 IEEE International Symposium on*, 1–6.

Sudatham, W., Matsumoto, H., Takahashi, S., and Takamasu, K. (2015). Verification of the positioning accuracy of industrial coordinate measuring machine using optical-comb pulsed interferometer with a rough metal ball target. *Precision Engineering*, 41, 63 – 67.

Yang, P., Takamura, T., Takahashi, S., Takamasu, K., Sato, O., Osawa, S., and Takatsuji, T. (2011). Development of high-precision micro-coordinate measuring machine: Multi-probe measurement system for measuring yaw and straightness motion error of XY linear stage. *Precision Engineering*, 35(3), 424 – 430.